

A New Type of High-Order WENO Schemes for Hamilton-Jacobi Equations on Triangular Meshes

Jun Zhu¹ and Jianxian Qiu^{2,*}

¹ College of Science, Nanjing University of Aeronautics and Astronautics, Nanjing, Jiangsu 210016, P.R. China.

² School of Mathematical Sciences and Fujian Provincial Key Laboratory of Mathematical Modeling and High-Performance Scientific Computation, Xiamen University, Xiamen, Fujian 361005, P.R. China.

Received 10 June 2018; Accepted (in revised version) 18 October 2018

Abstract. In this paper, a new type of third-order and fourth-order weighted essentially non-oscillatory (WENO) schemes is designed for simulating the Hamilton-Jacobi equations on triangular meshes. We design such schemes with the use of the nodal information defined on five unequal-sized spatial stencils, the application of monotone Hamiltonians as a building block, the artificial set of positive linear weights to make up high-order approximations in smooth regions simultaneously avoiding spurious oscillations nearby discontinuities of the derivatives of the solutions. The spatial reconstructions are convex combinations of the derivatives of a modified cubic/quartic polynomial defined on a big spatial stencil and four quadratic polynomials defined on small spatial stencils, and a third-order TVD Runge-Kutta method is used for the time discretization. The main advantages of these WENO schemes are their efficiency, simplicity, and can be easily implemented to higher dimensional unstructured meshes. Extensive numerical tests are performed to illustrate the good performance of such new WENO schemes.

AMS subject classifications: 65M60, 35L65

Key words: Unequal-sized stencil, weighted essentially non-oscillatory scheme, high-order approximation, Hamilton-Jacobi equation, triangular mesh.

1 Introduction

In this paper, we design a class of new third-order and fourth-order weighted essentially non-oscillatory (WENO) schemes for solving the Hamilton-Jacobi equations

$$\begin{cases} \phi_t + H(x, y, t, \phi, \phi_x, \phi_y) = 0, \\ \phi(x, y, 0) = \phi_0(x, y), \end{cases} \quad (1.1)$$

*Corresponding author. *Email addresses:* zhu jun@nuaa.edu.cn (J. Zhu), jxqiu@xmu.edu.cn (J. Qiu)

on triangular meshes. It is well known that the Hamilton-Jacobi (HJ) equations are often used in the applications of differential games, geometric optics, computer vision, variational calculus, control theory, etching, robotic navigation, and crystal growth [11, 33, 43]. The solution of (1.1) is continuous but the derivatives of the solution may have discontinuities or generate singularities via time approaching.

The concepts of the entropy conditions and the definition of the viscosity solution were formulated in [13–15, 47]. Abgrall and Sonar [2] pointed out that the viscosity solutions of the HJ equations may not be unique with the consideration of the physical implications. The HJ equations show very close relationship to the conservation laws and the numerical methods for HJ equation are similar to those for the conservation laws [4, 39, 40]. In 1984, Crandall and Lions [16] proposed first-order monotone finite difference schemes and then indicated that such schemes could converge to the viscosity solution of (1.1). Osher and Sethian [35] proposed a second-order essentially non-oscillatory (ENO) scheme for solving the HJ equations. Osher and Shu [36] designed high-order accurate ENO schemes for solving the HJ equations. Lafon and Osher [25] proposed unstructured ENO schemes for solving the HJ equations. In 2000, Jiang and Peng [21] proposed finite difference high-order weighted ENO (WENO) [22, 31, 34] scheme for solving the HJ equations on structured meshes which used the similar framework proposed by Jiang and Shu [22] for the conservation laws. Li and Chan [30], and Zhang and Shu [49] also proposed unstructured different finite difference high-order WENO schemes for solving the HJ equations in two dimensions. Herein, Qiu [37, 38], and Qiu and Shu [41] designed Hermite WENO (HWENO) schemes based on the finite volume and finite difference frameworks for solving the HJ equations on structured meshes. The central high resolution schemes for the HJ equations were presented by a series of literature, e.g. [7–9, 24, 27, 32]. Some schemes, such as weighted power ENO schemes [42], mapped WENO schemes [9, 18], discontinuous Galerkin schemes [12] and relaxation schemes [23] *et al.*, were also used to solve for the HJ equations. In [3, 5, 19, 26], some finite element methods were constructed on unstructured meshes. Hu and Shu [19] proposed discontinuous Galerkin methods for solving the HJ equations. In 2011, Yan and Osher [48] gave a local discontinuous Galerkin method for solving the HJ equations.

This paper is a new extension of [54] from finite volume schemes for the conservation laws to finite difference schemes for the HJ equations, based on the similar spirit of WENO methodologies specified in [49]. The major advantage of such new WENO schemes is their easy implementation in the computation. These new WENO schemes have convex combinations of x - or y -directional derivatives of one modified high degree polynomial and four low degree polynomials. The essential merits of such methodology are its robustness in spatial field by the definition of any positive linear weights, and only one central big spatial stencil and four biased or central small stencils are used to reconstruct five different degree polynomials. Therefore, we apply the derivatives of the high degree polynomial defined on central big spatial stencil for obtaining high-order numerical approximations of $\nabla\phi$ at different vertexes in smooth regions and switch to the derivatives of quadratic degree polynomials defined on biased or central small spa-

tial stencils near discontinuities. Thereafter, the new nonlinear weight formulas are presented for such five unequal degree polynomials on triangular meshes. Generally speaking, the primary innovations of this paper lie in three aspects: the new way to reconstruct x - and y -directional derivatives of one high degree polynomial and four quadratic polynomials, a robust WENO type communications among such five unequal degree polynomials for obtaining high-order approximations to the derivative quantities at different vertexes, and the new formulations of the nonlinear weights for unequal degree polynomials on triangular meshes.

The organization of the paper is as follows. In Section 2, we review and construct the new third-order and fourth-order accurate nodal based WENO schemes in detail for solving the HJ equations on triangular meshes and present extensive numerical results in Section 3 to verify the accuracy and easy implementation. Concluding remarks are given in Section 4.

2 The construction of WENO schemes for HJ equations

In this section, we give the framework of solving the HJ equations briefly and then develop the procedures of high-order WENO schemes for the HJ equations on triangular meshes.

2.1 The framework

We consider the governing equation (1.1) in the field Ω , which is partitioned into several non-overlapped triangles $\Delta_{\ell\ell}$, $\ell\ell = 1, \dots, N$. We define $\phi_i(t) = \phi(x_i, y_i, t)$ as the numerical approximation to the viscosity solution of (1.1) at vertex i of the triangle $\Delta_{\ell\ell}$ and abbreviate as ϕ_i in the following if it does not cause confusion. For every node i , we define the angular sectors T_0, \dots, T_{k_i} , which meet at vertex (x_i, y_i) . They are the inner angles defined at node i of the triangles which contain it as a vertex. The index of the angular sectors is ordered anticlockwise in this paper. $n_{\sigma+1/2}$ is the unit vector of the half-line $D_{\sigma+1/2} = T_\sigma \cap T_{\sigma+1}$, and θ_σ is the inner angle of sector T_σ , $0 \leq \sigma \leq k_i$ (see Fig. 1). So $\nabla\phi_0, \dots, \nabla\phi_{k_i}$ are the numerical approximations of $\nabla\phi$ at node i in each angular sector T_0, \dots, T_{k_i} , respectively. The two-dimensional governing equation is

$$\begin{cases} \frac{d}{dt}\phi_i(t) = -H(\nabla\phi_i), \\ \phi(x_i, y_i, 0) = \phi_0(x_i, y_i). \end{cases} \tag{2.1}$$

Then the right term of (2.1) is approximated by

$$\frac{d}{dt}\phi_i(t) = -\hat{H}_i = L(\phi_i). \tag{2.2}$$

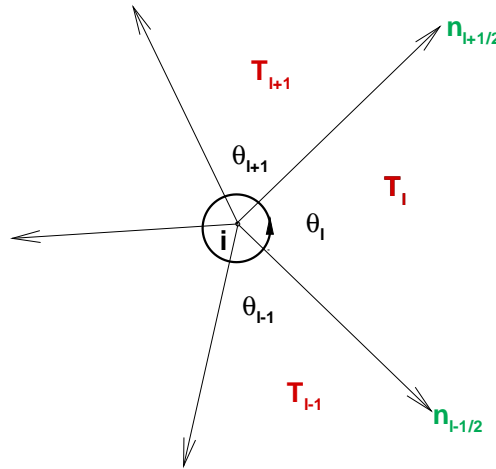


Figure 1: Node i and its inner angular sectors.

\hat{H}_i is a global Lax-Friedrichs monotone Hamiltonian [1, 36] (see Fig. 1) and is defined as

$$\hat{H}_i = H \left(\frac{\sum_{\sigma=0}^{k_i} \theta_{\sigma} (\nabla \phi_i)_{\sigma}}{2\pi} \right) - \frac{\alpha}{\pi} \sum_{\sigma=0}^{k_i} \beta_{\sigma+1/2} \left(\frac{(\nabla \phi_i)_{\sigma} + (\nabla \phi_i)_{\sigma+1}}{2} \right) \cdot n_{\sigma+1/2}, \quad (2.3)$$

where $\beta_{\sigma+1/2} = \tan(\frac{\theta_{\sigma}}{2}) + \tan(\frac{\theta_{\sigma+1}}{2})$. θ_{σ} , $\sigma = 0, \dots, k_i$ are the anticlockwise inner angle of sectors, and $\theta_{k_i} = \theta_0$. Then we set $\alpha = \max\{\alpha_x, \alpha_y\} = \max\{\max|H_1|, \max|H_2|\}$. Here H_1 and H_2 are the partial derivatives of H with respect to ϕ_x and ϕ_y , otherwise, are the Lipschitz constants of H globally (if they are not differentiable). If we could obtain high-order spatial nodal approximations of $\nabla \phi$ at node i in every angular sector, the numerical Hamiltonian H will get a high-order approximation with respect to H as defined in [49].

Then a third-order TVD Runge-Kutta time discretization method [46]

$$\begin{cases} \phi_i^{(1)} = \phi_i^n + \Delta t L(\phi_i^n), \\ \phi_i^{(2)} = \frac{3}{4}\phi_i^n + \frac{1}{4}\phi_i^{(1)} + \frac{1}{4}\Delta t L(\phi_i^{(1)}), \\ \phi_i^{n+1} = \frac{1}{3}\phi_i^n + \frac{2}{3}\phi_i^{(2)} + \frac{2}{3}\Delta t L(\phi_i^{(2)}), \end{cases} \quad (2.4)$$

is applied to obtain a full discretization scheme both in space and time. And the variable t in $\phi(x, y, t)$ is also omitted in the following if it does not cause confusion.

We now give the crucial procedures of two high-order finite difference WENO schemes using the point values ϕ_i defined on the vertexes to approximate the point values of $\nabla \phi$ at the same vertexes on triangular meshes. These reconstructions should be both high-order accurate in smooth regions and keep essentially non-oscillatory property near the discontinuities of the derivatives of the solutions. We take into account the procedures of third-order and fourth-order cases in the following.

2.2 The third-order spatial reconstruction

The third-order reconstructions of $\nabla(\phi)$ at the vertexes (x_ℓ, y_ℓ) , $\ell = i, j, k$ of the target cell Δ_0 (in the relevant angular sectors) are addressed in the following (see Figs. 1 and 2).

Step 1.1. Select a central spatial stencil containing at least ten nodes. For example (as shown in Fig. 2), we choose a target cell Δ_0 and form a spatial stencil $S_1 = \{1, 2, 3\}$ (nodes 1, 2, 3 coincide with nodes i, j, k , respectively). Then we search three immediate neighboring triangles of Δ_0 as $\Delta_{01}, \Delta_{02}, \Delta_{03}$ and add new nodes (which are the vertexes of these triangles) to S_1 and form the spatial stencil $S_1 \equiv S_1 \cup \{4, \dots, N_1\}$, where $5 \leq N_1 \leq 6$. After that, we search the neighboring triangles of such three triangles as $\Delta_{011}, \Delta_{012}, \Delta_{021}, \Delta_{022}, \Delta_{031}$, and Δ_{032} (some of them may coincide with each other), add new vertexes of these triangles to S_1 , and form the spatial stencil $S_1 \equiv S_1 \cup \{N_1 + 1, \dots, N_2\}$. If $10 \leq N_2$, we can use these N_2 point values to reconstruct a cubic polynomial. Otherwise, such as shown in Fig. 2, we need to search new triangles of the next layer of such triangles as $\Delta_{0111}, \Delta_{0112}, \Delta_{0121}, \Delta_{0122}, \Delta_{0211}, \Delta_{0212}, \Delta_{0221}, \Delta_{0222}, \Delta_{0311}, \Delta_{0312}, \Delta_{0321}$, and Δ_{0322} (some of them may coincide with each other once again), respectively. Then we could add new vertexes of such triangles to S_1 and form the nodal spatial stencil $S_1 \equiv S_1 \cup \{N_2 + 1, \dots, N_3\}$. Such procedure is fulfilled sequentially until the big nodal stencil S_1 contains at least ten nodes for the spatial reconstruction. It is well known that the interpolating polynomial based on the information on such nodes is not always easy to be solved. Associated linear system to calculate the polynomial can be an ill-conditioned problem or a singular problem, such that we need to add new nodes to the chosen central spatial stencil from the neighboring triangles around the target triangle Δ_0 and its immediate neighbors, so as to form a new

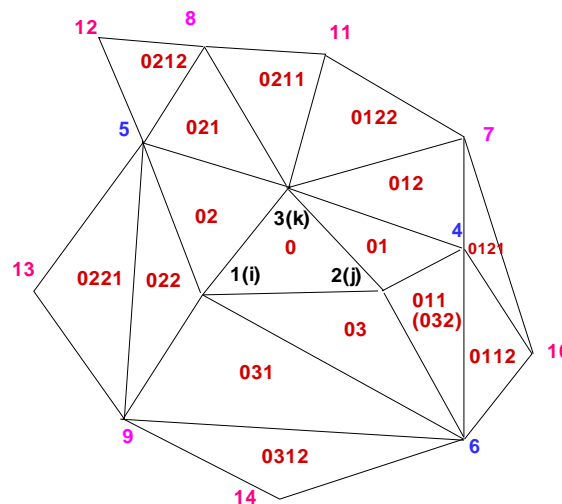


Figure 2: The first type of central spatial stencil.

linear system. We remark that this ill-conditioned problem comes from both the geometric distribution of the nodes, for which we could do nothing but change the nodes of the computing mesh, and from the choice of basis functions in the interpolation [49]. Then we construct a cubic polynomial

$$q_1(x,y) \in span \left\{ 1, \frac{(x-x_0)}{\sqrt{|\Delta_0|}}, \frac{(y-y_0)}{\sqrt{|\Delta_0|}}, \frac{(x-x_0)^2}{|\Delta_0|}, \frac{(x-x_0)(y-y_0)}{|\Delta_0|}, \frac{(y-y_0)^2}{|\Delta_0|}, \frac{(x-x_0)^3}{\sqrt{|\Delta_0|^3}}, \frac{(x-x_0)^2(y-y_0)}{\sqrt{|\Delta_0|^3}}, \frac{(x-x_0)(y-y_0)^2}{\sqrt{|\Delta_0|^3}}, \frac{(y-y_0)^3}{\sqrt{|\Delta_0|^3}} \right\}$$

by requiring it has the same point values of ϕ at nodes 1, 2, 3, and matches the same point values of ϕ in the set $A = S_1 \setminus \{1,2,3\}$ in a least square sense [19,20,49]:

$$q_1(x_\ell, y_\ell) = \phi(x_\ell, y_\ell), \quad \ell = 1, 2, 3, \tag{2.5}$$

and

$$\min_{\ell \in A} \sum (q_1(x_\ell, y_\ell) - \phi(x_\ell, y_\ell))^2, \quad A = S_1 \setminus \{1, 2, 3\}. \tag{2.6}$$

Then the reconstructed polynomial $\nabla q_1(x,y)$ will be a third-order approximation to $\nabla \phi$ over Δ_0 .

Step 1.2. Select three small biased stencils and one small central stencil. For example (as shown in Fig. 2), We choose three biased stencils S_2, S_3, S_4 , and one central stencil S_5 , which contain the vertexes of $\Delta_{\ell\ell}, \ell\ell = 0,01,011,012; \ell\ell = 0,02,021,022; \ell\ell = 0,03,031,032$ and $\ell\ell = 0,01,02,03$, respectively. And we should confirm a fact that each of them contains at least six distinct nodes (otherwise, the vertexes of the neighboring triangles of $\Delta_{\ell\ell}, \ell\ell = 011,012; \ell\ell = 021,022; \ell\ell = 031,032$ and $\ell\ell = 01,02,03$ are added to associated stencils $S_l, l = 2, \dots, 5$ if necessary, and such searching algorithm can be fulfilled sequentially until each of these stencils contains enough nodes). Then we construct quadratic polynomials $q_l(x,y) \in span \{1, \frac{(x-x_0)}{\sqrt{|\Delta_0|}}, \frac{(y-y_0)}{\sqrt{|\Delta_0|}}, \frac{(x-x_0)^2}{|\Delta_0|}, \frac{(x-x_0)(y-y_0)}{|\Delta_0|}, \frac{(y-y_0)^2}{|\Delta_0|}\}, l = 2, \dots, 5$ by requiring

$$q_l(x_\ell, y_\ell) = \phi(x_\ell, y_\ell), \quad \ell = 1, 2, 3, \\ \min_{\ell \in A_l} \sum (q_l(x_\ell, y_\ell) - \phi(x_\ell, y_\ell))^2, \quad A_l = S_l \setminus \{1, 2, 3\}, \quad l = 2, \dots, 5. \tag{2.7}$$

Remark 2.1. We apply the values of at least six nodes for constructing quadratic polynomials $q_l(x,y), l = 2, \dots, 5$, since each of them has six degrees of freedom. We should choose at least three nodes from the neighboring triangles of the target triangle Δ_0 , other than node 1 (target node i), node 2 (node j), and node 3 (node k). For example (as shown in Fig. 2), we choose such three biased stencils $S_2 = \{1,2,3,4,6,7\}, S_3 = \{1,2,3,5,8,9\}$, and $S_4 = \{1,2,3,4,6,9\}$, respectively. By doing so, we could keep essentially non-oscillatory property of the scheme in case that there are discontinuities. And we could also maintain such property by applying a central stencil $S_5 = \{1,2,3,4,5,6\}$ which is often wrongly

omitted. Such four small spatial stencils (three small biased stencils and one small central stencil) are indispensable here. And we would like to point out a fact that the nodes on such small stencils $S_l, l=2, \dots, 5$ do not need to coincide with the nodes in the big stencil S_1 .

Step 1.3. Set any positive linear weights $\gamma_1, \dots, \gamma_5$ with one requirement $\sum_{\kappa=1}^5 \gamma_\kappa = 1$. With the similar idea in [28,29], we rewrite $\nabla q_1(x,y)$ as

$$\nabla q_1(x,y) = \gamma_1 \left(\frac{1}{\gamma_1} \nabla q_1(x,y) - \sum_{\kappa=2}^5 \frac{\gamma_\kappa}{\gamma_1} \nabla q_\kappa(x,y) \right) + \sum_{\kappa=2}^5 \gamma_\kappa \nabla q_\kappa(x,y). \quad (2.8)$$

In this paper, following the practice in [17, 50–53, 55, 56], one type of such linear weights is defined as $\gamma_1=0.96$ and $\gamma_2=\gamma_3=\gamma_4=\gamma_5=0.01$.

Step 1.4. We compute the smoothness indicators $\beta_l, l=1, \dots, 5$ which measure how smooth the functions $q_l(x,y), l=1, \dots, 5$ are in the triangle Δ_0 . The smaller these smoothness indicators, the smoother the functions are in the triangle Δ_0 . We use the similar recipe for the smoothness indicators as in [19, 22]:

$$\beta_l = \sum_{|\ell| \geq 2} \int_{\Delta_0} |\Delta_0|^{|\ell|-2} \left(\frac{\partial^{|\ell|}}{\partial x^{\ell_1} \partial y^{\ell_2}} q_l(x,y) \right)^2 dx dy, \quad l=1, \dots, 5, \quad (2.9)$$

where $\ell = (\ell_1, \ell_2)$ and $|\ell| = \ell_1 + \ell_2$. Their expansions in Taylor series at (x_0, y_0) of the barycenter of the target triangle Δ_0 are

$$\beta_1 = \left(\sum_{|\ell|=2} \left(\frac{\partial^{|\ell|}}{\partial x^{\ell_1} \partial y^{\ell_2}} \phi(x,y) \Big|_{(x_0,y_0)} \right)^2 \right) |\Delta_0| (1 + \mathcal{O}(|\Delta_0|)) = \mathcal{O}(|\Delta_0|), \quad (2.10)$$

and

$$\beta_l = \left(\sum_{|\ell|=2} \left(\frac{\partial^{|\ell|}}{\partial x^{\ell_1} \partial y^{\ell_2}} \phi(x,y) \Big|_{(x_0,y_0)} \right)^2 \right) |\Delta_0| (1 + \mathcal{O}(|\Delta_0|^{\frac{1}{2}})) = \mathcal{O}(|\Delta_0|), \quad l=2, \dots, 5. \quad (2.11)$$

Step 1.5. Compute the nonlinear weights based on the linear weights and the smoothness indicators. For instance, we use τ [51] which is simply defined as the absolute difference between $\beta_1, \beta_2, \beta_3, \beta_4,$ and β_5 , and is similar to that in [6, 10]. The difference expansions in Taylor series at (x_0, y_0) are

$$\beta_1 - \beta_l = \mathcal{O}(|\Delta_0|^{\frac{3}{2}}), \quad l=2, \dots, 5. \quad (2.12)$$

So it satisfies

$$\tau = \left(\frac{|\beta_1 - \beta_2| + |\beta_1 - \beta_3| + |\beta_1 - \beta_4| + |\beta_1 - \beta_5|}{4} \right)^2 = \mathcal{O}(|\Delta_0|^3). \quad (2.13)$$

Then the associated nonlinear weights are defined as

$$\omega_l = \frac{\bar{\omega}_l}{\sum_{\kappa=1}^5 \bar{\omega}_\kappa}, \quad \bar{\omega}_l = \gamma_l \left(1 + \frac{\tau}{\varepsilon + \beta_l} \right), \quad l=1, \dots, 5. \quad (2.14)$$

Here ε is a small positive number to avoid the denominator of (2.14) to become zero. By the implementation of (2.13) in smooth regions, they satisfy

$$\frac{\tau}{\varepsilon + \beta_l} = \mathcal{O}(|\Delta_0|^2), \quad l=1, \dots, 5, \quad (2.15)$$

on condition that $\varepsilon \ll \beta_l$. Therefore, the nonlinear weights ω_l , $l=1, \dots, 5$ satisfy the order accuracy condition $\omega_l = \gamma_l + \mathcal{O}(|\Delta_0|)$ [6, 10], providing the third-order accuracy to the WENO schemes narrated in [22, 45]. We set $\varepsilon = 10^{-6}$ in all simulations in this paper.

Step 1.6. The final reconstruction formulation of $\nabla\phi$ in the target cell Δ_0 is given by

$$\nabla\phi(x, y) \approx \omega_1 \left(\frac{1}{\gamma_1} \nabla q_1(x, y) - \sum_{\kappa=2}^5 \frac{\gamma_\kappa}{\gamma_1} \nabla q_\kappa(x, y) \right) + \sum_{\kappa=2}^5 \omega_\kappa \nabla q_\kappa(x, y), \quad (2.16)$$

and $\nabla\phi$ at vertexes i, j, k of the target cell Δ_0 are given by

$$\nabla(\phi_\ell) \approx \omega_1 \left(\frac{1}{\gamma_1} \nabla q_1(x_\ell, y_\ell) - \sum_{\kappa=2}^5 \frac{\gamma_\kappa}{\gamma_1} \nabla q_\kappa(x_\ell, y_\ell) \right) + \sum_{\kappa=2}^5 \omega_\kappa \nabla q_\kappa(x_\ell, y_\ell), \quad \ell = i, j, k. \quad (2.17)$$

Remark 2.2. There are two major advantages in this paper. The first, we only use five unequal degree polynomials defined on associated unequal-sized spatial stencils for the reconstruction, the linear weights are independent of the meshes and can be any positive numbers with only one requirement that their summation is one, in comparison with the sophisticated computations of the linear weights specified in [49] et al.. The second, we only need to compute the nonlinear weights one time for the vertexes i, j, k of the target cell Δ_0 and the nonlinear weights specified in [49] need to be computed for each vertex.

2.3 The fourth-order spatial reconstruction

The fourth-order reconstructions of $\nabla(\phi)$ at the vertexes (x_ℓ, y_ℓ) , $\ell = i, j, k$ of the target cell Δ_0 (in the relevant angular sectors) are addressed in the following (see Figs. 1 and 3).

Step 2.1. Select a central spatial stencil containing at least fifteen nodes. For example, as shown in Fig. 3, we also choose the target triangle Δ_0 including the target node i and other two nodes j, k as before. Then we apply the previous triangles and apply their vertexes to form a spatial stencil $S_1 = \{1, 2, 3, \dots, N_3\}$. If N_3 is less than fifteen, we should search other immediate neighboring triangles other than that mentioned above. Similarly, we should renumber vertexes of triangles Δ_{01111} , Δ_{01112} , Δ_{01121} , Δ_{01122} , Δ_{01211} , Δ_{01212} , Δ_{01221} , Δ_{01222} , Δ_{02111} , Δ_{02112} , Δ_{02121} , Δ_{02122} , Δ_{02211} , Δ_{02212} , Δ_{02221} , Δ_{02222} , Δ_{03111} , Δ_{03112} , Δ_{03121} ,

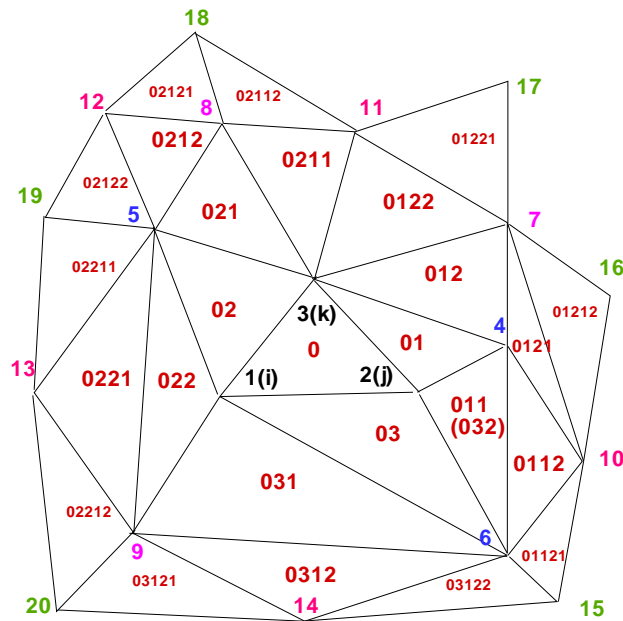


Figure 3: The second type of central spatial stencil.

Δ_{03122} , Δ_{03211} , Δ_{03212} , Δ_{03221} , Δ_{03222} (some of them coincide with each other), and add new vertexes of these triangles to S_1 and form a big stencil as $S_1 \equiv S_1 \cup \{N_3 + 1, \dots, N_4\}$ and confirm that N_4 is no less than fifteen. Then we construct a quartic polynomial

$$q_1(x,y) \in span \left\{ 1, \frac{(x-x_0)}{\sqrt{|\Delta_0|}}, \frac{(y-y_0)}{\sqrt{|\Delta_0|}}, \frac{(x-x_0)^2}{|\Delta_0|}, \frac{(x-x_0)(y-y_0)}{|\Delta_0|}, \frac{(y-y_0)^2}{|\Delta_0|}, \frac{(x-x_0)^3}{\sqrt{|\Delta_0|^3}}, \frac{(x-x_0)^2(y-y_0)}{\sqrt{|\Delta_0|^3}}, \frac{(x-x_0)(y-y_0)^2}{\sqrt{|\Delta_0|^3}}, \frac{(y-y_0)^3}{\sqrt{|\Delta_0|^3}}, \frac{(x-x_0)^4}{|\Delta_0|^2}, \frac{(x-x_0)^3(y-y_0)}{|\Delta_0|^2}, \frac{(x-x_0)^2(y-y_0)^2}{|\Delta_0|^2}, \frac{(x-x_0)(y-y_0)^3}{|\Delta_0|^2}, \frac{(y-y_0)^4}{|\Delta_0|^2} \right\}$$

by requiring it has the same point values of ϕ at nodes 1, 2, 3 (nodes i, j, k), and matches the same point values of ϕ in the set $S_1 \setminus \{1,2,3\}$ in a least square sense [19,20,49]:

$$q_1(x_\ell, y_\ell) = \phi(x_\ell, y_\ell), \quad \ell = 1, 2, 3, \tag{2.18}$$

and

$$\min \sum_{\ell \in A} (q_1(x_\ell, y_\ell) - \phi(x_\ell, y_\ell))^2, \quad A = S_1 \setminus \{1, 2, 3\}. \tag{2.19}$$

Then the reconstructed polynomial $\nabla q_1(x,y)$ will be a fourth-order approximation to $\nabla \phi$ over Δ_0 . We obey the same renumbering principle of all necessary nodes [49]. Since only three nodes are distinct points in Fig. 3, it is very crucial to rank and detect at least

fifteen distinct nodes in spatial stencil S_1 for constructing the quartic polynomial $q_1(x, y)$. Otherwise, the stencil S_1 might not contain enough nodes for designing the fourth-order reconstruction and new nodes lie in neighboring triangles around the target triangle Δ_0 and its neighbors are searched sequentially.

Step 2.2. Select three biased and one central stencils $S_l, l=2, \dots, 5$ which are the same as those noted in Step 1.2, and then construct four quadratic polynomials $q_l(x, y), l=2, \dots, 5$.

Step 2.3. Set any positive linear weights $\gamma_1, \dots, \gamma_5$ with the same restriction as in Step 1.3.

Step 2.4. Compute the smoothness indicators by (2.9). Their expansions in Taylor series at (x_0, y_0) of the barycenter of the target triangle Δ_0 are

$$\beta_1 = \left(\sum_{|\ell|=2} \left(\frac{\partial^{|\ell|}}{\partial x^{\ell_1} \partial y^{\ell_2}} \phi(x, y) \Big|_{(x_0, y_0)} \right)^2 \right) |\Delta_0| (1 + \mathcal{O}(|\Delta_0|^{\frac{3}{2}})) = \mathcal{O}(|\Delta_0|), \quad (2.20)$$

and $\beta_l, l=2, \dots, 5$ are given in (2.11).

Step 2.5. Compute the nonlinear weights. The difference expansions in Taylor series at (x_0, y_0) are (2.12) and satisfy (2.13). Then associate nonlinear weights are defined as (2.14). By the implementation of (2.13) in smooth regions, they satisfy (2.15). Therefore, the nonlinear weights $\omega_l, l=1, \dots, 5$ satisfy the order accuracy requirement $\omega_l = \gamma_l + \mathcal{O}(|\Delta_0|^{\frac{3}{2}})$ [6, 10], providing the fourth-order accuracy to the WENO schemes [22, 45].

Step 2.6. The new final reconstruction formulations of $\nabla \phi$ at vertexes i, j, k of the target cell Δ_0 are also given as narrated in (2.17).

Remark 2.3. Roughly speaking, to construct the third-order and fourth-order WENO schemes, we need to find a big central spatial stencil S_1 containing enough distinct nodes and keep nodes 1, 2, and 3 in all stencils $S_l, l=1, \dots, 5$. We also need to confirm these nodes are central in the big stencil S_1 , so as to avoid S_1 to be seriously downwind biased, which might result in the appearance of linear instability [49]. One crucial innovation in this paper is the application of x - and y -directional derivatives using only five unequal degree polynomials to approximate $\nabla \phi$ at vertexes of all triangles avoiding the sophisticated calculation of different types of optimal linear weights. Such new WENO schemes use the derivatives of a high degree polynomial to obtain high-order approximation at any nodes in smooth regions and switch to the derivatives of either of four low degree polynomials to keep essentially non-oscillatory property in non-smooth regions.

3 Numerical tests

In this section, we present the results of numerical tests for third-order and fourth-order WENO schemes which are termed as WENO3 and WENO4 schemes, respectively. The CFL number is 0.6. For the temporal discretization, the third-order TVD Runge-Kutta time discretization method [46] is used here for all examples. Only for the accuracy tests,

we set time step as $\Delta t = \min_{\ell} (|\Delta_{\ell}|^{\frac{1}{2}})^{\frac{\kappa}{3}}$, and $\kappa = 3$ (for the third-order WENO scheme) or $\kappa = 4$ (for the fourth-order WENO scheme) to confirm that spatial error dominates. Otherwise, we recover $\kappa = 3$ for other examples in this paper. For the sake of evaluating whether the random choice of the linear weights would pollute the optimal order accuracy of such new WENO schemes or not, we set four different types of linear weights in the numerical accuracy examples as: (1) $\gamma_1 = 0.96$ and $\gamma_2 = \gamma_3 = \gamma_4 = \gamma_5 = 0.01$; (2) $\gamma_1 = \gamma_2 = \gamma_3 = \gamma_4 = \gamma_5 = 0.2$; (3) $\gamma_1 = 0.01$ and $\gamma_2 = \gamma_3 = \gamma_4 = \gamma_5 = 0.2475$; (4) $\gamma_1 = \gamma_2 = \gamma_3 = \gamma_4 = 0.01$ and $\gamma_5 = 0.96$. And then we apply the first type of the linear weights for the latter examples, unless specified otherwise.

Example 3.1. We solve the following HJ equation [30]:

$$\phi_t - \cos(\phi_x + \phi_y + 1) = 0, \quad -2 \leq x, y < 2, \tag{3.1}$$

with the initial condition $\phi(x, y, 0) = -\cos(\pi(x+y)/2)$ and the periodic boundary conditions in two directions. When $t = 0.5/\pi^2$ the solution is still smooth. A sample mesh with boundary triangle size $h = 0.4$ is shown in Fig. 4. The errors and orders of accuracy by WENO3 and WENO4 schemes are shown in Table 1. We can see that both schemes achieve their designed order of accuracy.

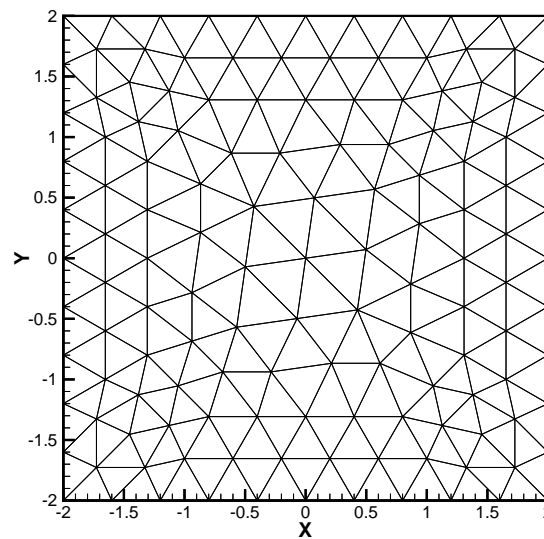


Figure 4: The sample mesh.

Example 3.2. We solve the following two dimensional Burgers' equation:

$$\phi_t + \frac{(\phi_x + \phi_y + 1)^2}{2} = 0, \quad -2 \leq x, y < 2, \tag{3.2}$$

Table 1: $\phi_t - \cos(\phi_x + \phi_y + 1) = 0$. $\phi(x, y, 0) = -\cos(\pi(x+y)/2)$. Periodic boundary conditions. $T = 0.5/\pi^2$.

	WENO3 (1)				WENO3 (2)			
points	L^1 error	order	L^∞ error	order	L^1 error	order	L^∞ error	order
137	2.31E-3		7.10E-3		4.14E-3		1.40E-2	
505	4.13E-4	2.49	2.15E-3	1.72	4.79E-4	3.11	3.17E-3	2.15
1937	6.40E-5	2.69	4.98E-4	2.11	6.41E-5	2.90	4.98E-4	2.67
7585	8.32E-6	2.94	9.12E-5	2.45	8.32E-6	2.95	9.12E-5	2.45
30017	1.03E-6	3.00	1.20E-5	2.92	1.03E-6	3.00	1.20E-5	2.92
	WENO3 (3)				WENO3 (4)			
points	L^1 error	order	L^∞ error	order	L^1 error	order	L^∞ error	order
137	4.43E-3		1.48E-2		3.76E-3		9.81E-3	
505	4.94E-4	3.16	3.45E-3	2.10	4.72E-4	2.99	2.25E-3	2.12
1937	6.43E-5	2.94	4.98E-4	2.79	6.44E-5	2.87	4.98E-4	2.18
7585	8.32E-6	2.95	9.12E-5	2.45	8.32E-6	2.95	9.12E-5	2.45
30017	1.03E-6	3.00	1.20E-5	2.92	1.03E-6	3.00	1.20E-5	2.92
	WENO4 (1)				WENO4 (2)			
points	L^1 error	order	L^∞ error	order	L^1 error	order	L^∞ error	order
137	1.84E-3		8.57E-3		3.49E-3		1.33E-2	
505	2.38E-4	2.95	1.14E-3	2.90	3.06E-4	3.51	3.03E-3	2.14
1937	2.00E-5	3.57	1.70E-4	2.75	2.10E-5	3.86	1.71E-4	4.15
7585	1.11E-6	4.17	1.77E-5	3.26	1.12E-6	4.23	1.77E-5	3.27
30017	4.61E-8	4.59	9.89E-7	4.16	4.61E-8	4.60	9.89E-7	4.16
	WENO4 (3)				WENO4 (4)			
points	L^1 error	order	L^∞ error	order	L^1 error	order	L^∞ error	order
137	3.77E-3		1.43E-2		2.66E-3		8.42E-3	
505	3.21E-4	3.55	3.31E-3	2.11	2.96E-4	3.17	1.31E-3	2.68
1937	2.13E-5	3.91	1.71E-4	4.27	2.11E-5	3.81	1.71E-4	2.94
7585	1.12E-6	4.25	1.77E-5	3.28	1.11E-6	4.24	1.77E-5	3.27
30017	4.61E-8	4.60	9.89E-7	4.16	4.61E-8	4.60	9.89E-7	4.16

with the initial condition $\phi(x, y, 0) = -\cos(\pi(x+y)/2)$ and periodic boundary conditions in two directions. When $t = 0.5/\pi^2$ the solution is still smooth. The same sample mesh with boundary triangle size $h = 0.4$ is also shown in Fig. 4. The errors and orders of accuracy by two new WENO schemes are shown in Table 2 and the numerical errors against number of points graphs are presented in Fig. 5. We can observe that the optimal order of accuracy is actually achieved and WENO schemes can get better results than that of WENO-ZS schemes in [49] for this two-dimensional test case.

Table 2: $\phi_t + \frac{(\phi_x + \phi_y + 1)^2}{2} = 0$. $\phi(x, y, 0) = -\cos(\pi(x+y)/2)$. Periodic boundary conditions. $T = 0.5/\pi^2$.

		WENO3 (1)				WENO3 (2)			
points	L^1 error	order	L^∞ error	order	L^1 error	order	L^∞ error	order	
137	1.00E-2		3.11E-2		1.72E-2		6.92E-2		
505	1.15E-3	3.12	4.21E-3	2.89	1.31E-3	3.72	5.47E-3	3.66	
1937	1.43E-4	3.00	5.76E-4	2.87	1.40E-4	3.22	5.76E-4	3.25	
7585	1.75E-5	3.03	7.20E-5	3.00	1.75E-5	3.00	7.20E-5	3.00	
30017	2.17E-6	3.01	8.98E-6	3.00	2.17E-6	3.01	8.98E-6	3.00	
		WENO3 (3)				WENO3 (4)			
points	L^1 error	order	L^∞ error	order	L^1 error	order	L^∞ error	order	
137	1.80E-2		7.12E-2		1.46E-2		6.11E-2		
505	1.39E-3	3.69	6.01E-3	3.57	1.24E-3	3.56	5.32E-3	3.52	
1937	1.39E-4	3.32	5.77E-4	3.38	1.42E-4	3.13	5.76E-4	3.21	
7585	1.75E-5	2.99	7.20E-5	3.00	1.75E-5	3.02	7.20E-5	3.00	
30017	2.17E-6	3.01	8.98E-6	3.00	2.17E-6	3.01	8.98E-6	3.00	
		WENO4 (1)				WENO4 (2)			
points	L^1 error	order	L^∞ error	order	L^1 error	order	L^∞ error	order	
137	5.14E-3		3.19E-2		1.34E-2		6.67E-2		
505	2.36E-4	4.45	3.92E-3	3.02	6.21E-4	4.44	4.14E-3	4.01	
1937	1.05E-5	4.49	4.01E-4	3.29	1.41E-5	5.45	4.07E-4	3.35	
7585	4.00E-7	4.72	3.10E-5	3.69	4.09E-7	5.11	3.10E-5	3.71	
30017	1.49E-8	4.74	2.07E-6	3.90	1.48E-8	4.78	2.07E-6	3.90	
		WENO4 (3)				WENO4 (4)			
points	L^1 error	order	L^∞ error	order	L^1 error	order	L^∞ error	order	
137	1.43E-2		6.84E-2		9.85E-3		5.43E-2		
505	7.29E-4	4.30	4.75E-3	3.85	4.62E-4	4.41	4.10E-3	3.73	
1937	1.53E-5	5.57	4.08E-4	3.54	1.43E-5	5.01	4.07E-4	3.33	
7585	4.15E-7	5.21	3.10E-5	3.72	4.16E-7	5.10	3.10E-5	3.71	
30017	1.48E-8	4.80	2.07E-6	3.90	1.49E-8	4.80	2.07E-6	3.90	

Example 3.3. We solve one-dimensional Burgers' equation:

$$\phi_t + \frac{(\phi_x + 1)^2}{2} = 0, \quad -1 \leq x \leq 1, \tag{3.3}$$

with the initial condition $\phi(x, 0) = -\cos(\pi x)$ and periodic boundary condition. We consider the solution of (3.3) in a domain of $[-1, 1] \times [-0.25, 0.25]$ (see Fig. 6) with a triangulation of 41 vertices in x - and y -direction. Periodic boundary condition is used in the y -direction. We plot the results at $t = 3.5/\pi^2$ when discontinuous derivative appears. The

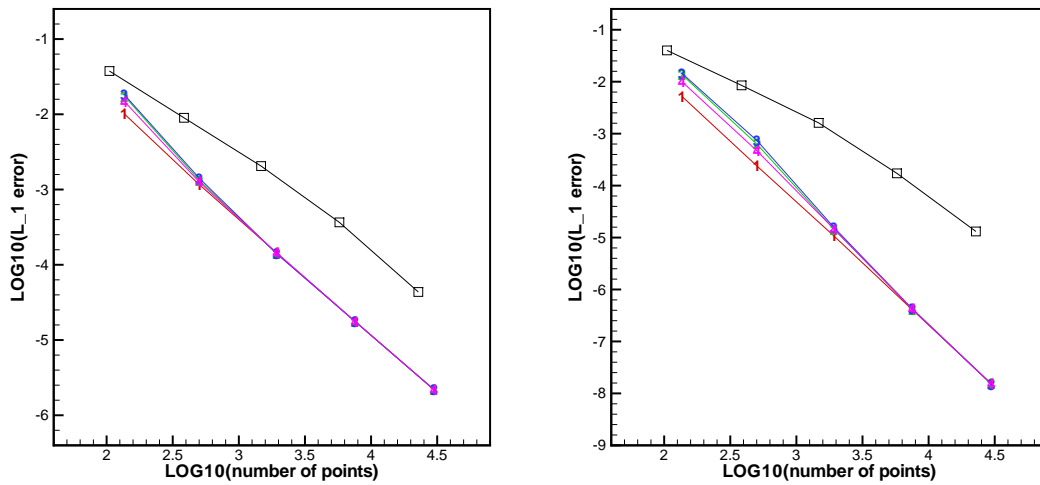


Figure 5: $\phi_t + \frac{(\phi_x + \phi_y + 1)^2}{2} = 0$. $\phi(x, y, 0) = -\cos(\pi(x+y)/2)$. Number of points and error. Number signs and a solid line denote the results of WENO scheme with different linear weights (1), (2), (3), and (4); squares and a solid line denote the results of WENO-ZS scheme in [49]. Left: WENO3 and WENO3-ZS scheme; right: WENO4 and WENO4-ZS scheme.

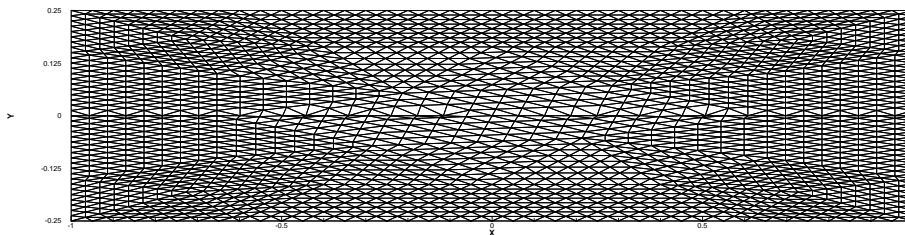


Figure 6: One-dimensional Burgers' equation. The sample mesh.

pictures shown below in Fig. 7 are obtained by extracting the data along the central cut line $y=0$. We can see the schemes give good results for this problem.

Example 3.4. We solve the nonlinear equation with a non-convex flux:

$$\phi_t - \cos(\phi_x + 1) = 0, \quad -1 \leq x \leq 1, \tag{3.4}$$

with the initial data $\phi(x, 0) = -\cos(\pi x)$ and periodic boundary condition. We consider the solution of (3.4) in the same domain of $[-1, 1] \times [-0.25, 0.25]$ (see Fig. 6) with a triangulation of 41 vertices in x - and y -direction. Periodic boundary condition is used in the y -direction. Then we plot the results at $t = 1.5/\pi^2$ in Fig. 8 when the discontinuous derivative appears in the solution. The pictures shown in Fig. 8 are obtained by extracting the data along the central cut line $y = 0$. We can see that two WENO schemes give good results for this problem once again.

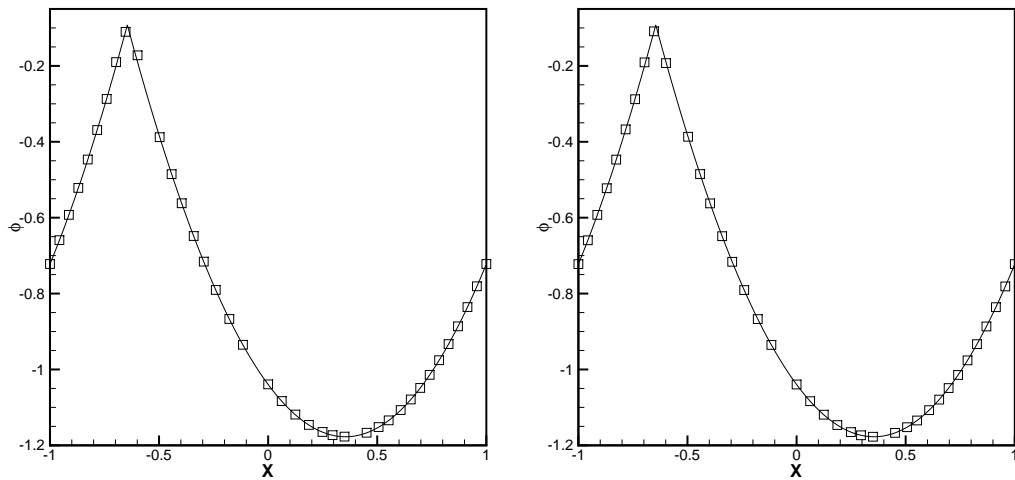


Figure 7: One-dimensional Burgers' equation. Boundary triangle size $h = \frac{2}{40}$ in x -direction. $T = 3.5/\pi^2$. Solid line: the exact solution; square symbols: WENO scheme. Left: WENO3 scheme; right: WENO4 scheme.

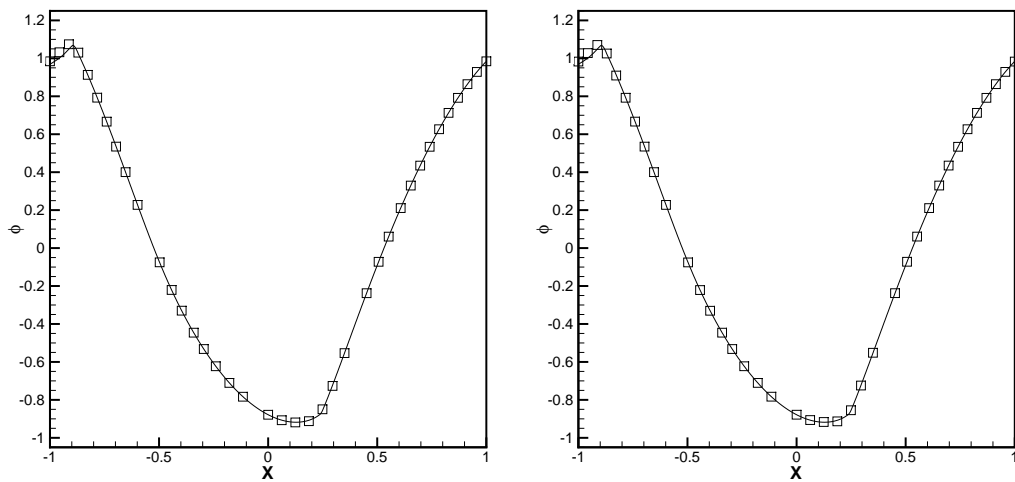


Figure 8: Problem with the non-convex flux $H(\phi_x) = -\cos(\phi_x + 1)$. Boundary triangle size $h = \frac{2}{40}$ in x -direction. $T = 1.5/\pi^2$. Solid line: the exact solution; square symbols: WENO scheme. Left: WENO3 scheme; right: WENO4 scheme.

Example 3.5. We solve the same two dimensional Burgers' equation (3.2) as in Example 3.2 with the same initial condition $\phi(x, y, 0) = -\cos(\pi(x+y)/2)$, except that we now plot the results at $t = 1.5/\pi^2$ with boundary triangle size $h = 0.1$ (see Fig. 9) in Fig. 10 and Fig. 11, respectively, when the discontinuous derivative has already appeared in the solution. We observe that two new WENO schemes could get good resolutions for this example.

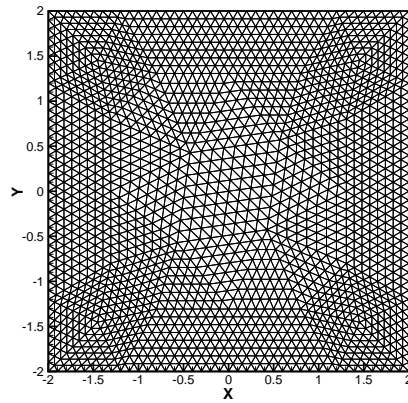


Figure 9: Two dimensional Burgers' equation. The sample mesh.

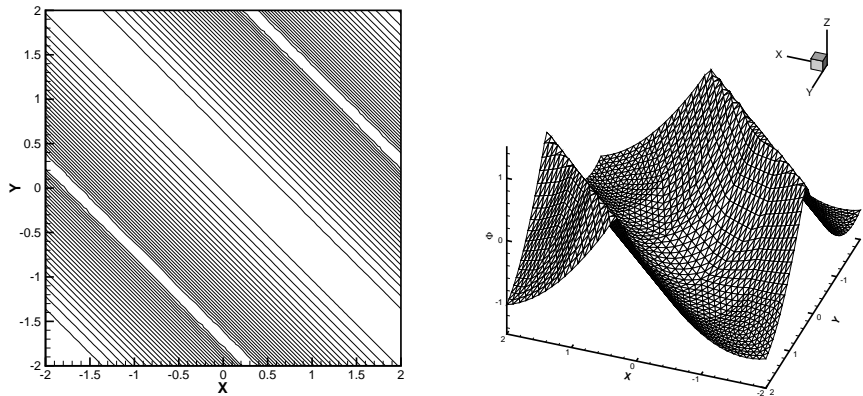


Figure 10: Two dimensional Burgers' equation. Boundary triangle size: $h=0.1$. $T=1.5/\pi^2$. WENO3 scheme. Left: contours of the solution; right: the surface of the solution.

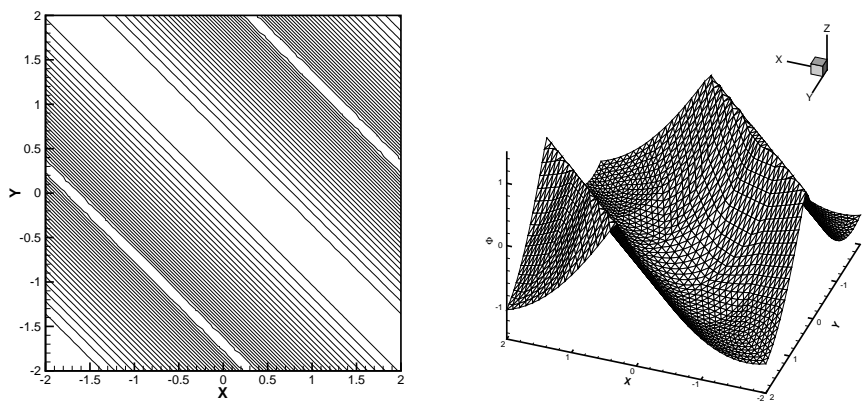


Figure 11: Two dimensional Burgers' equation. Boundary triangle size: $h=0.1$. $T=1.5/\pi^2$. WENO4 scheme. Left: contours of the solution; right: the surface of the solution.

Example 3.6. The two dimensional Riemann problem with a non-convex flux:

$$\begin{cases} \phi_t + \sin(\phi_x + \phi_y) = 0, & -1 \leq x, y < 1, \\ \phi(x, y, 0) = \pi(|y| - |x|). \end{cases} \quad (3.5)$$

The solution of the WENO3 and WENO4 schemes plotted at $t=1$ with boundary triangle size $h = 0.05$ (see Fig. 9) are shown in Fig. 12 and Fig. 13. We can also observe good resolutions of these schemes.

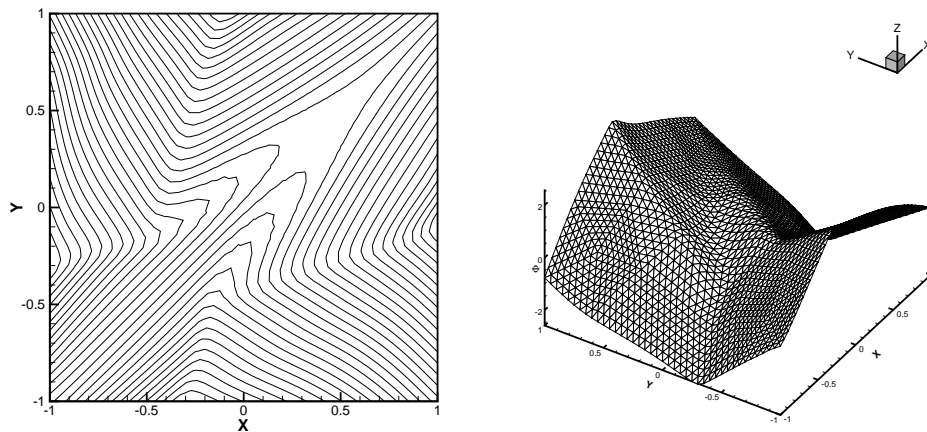


Figure 12: Two dimensional Riemann problem with a non-convex flux $H(\phi_x, \phi_y) = \sin(\phi_x + \phi_y)$. Boundary triangle size: $h=0.05$. $T=1$. WENO3 scheme. Left: contours of the solution; right: the surface of the solution.

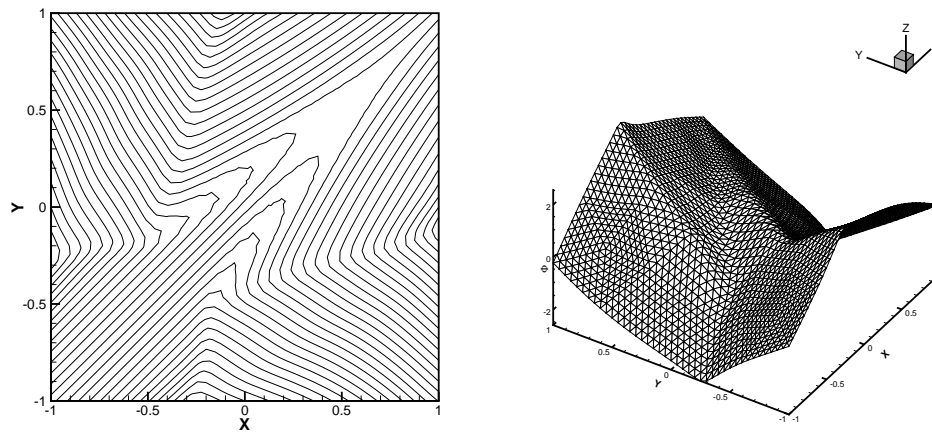


Figure 13: Two dimensional Riemann problem with a non-convex flux $H(\phi_x, \phi_y) = \sin(\phi_x + \phi_y)$. Boundary triangle size: $h=0.05$. $T=1$. WENO4 scheme. Left: contours of the solution; right: the surface of the solution.

Example 3.7. A problem from optimal control:

$$\begin{cases} \phi_t + \sin(y)\phi_x + (\sin(x) + \text{sign}(\phi_y))\phi_y - \frac{1}{2}\sin(y)^2 - (1 - \cos(x)) = 0, & -\pi \leq x, y < \pi, \\ \phi(x, y, 0) = 0, \end{cases} \quad (3.6)$$

with periodic boundary conditions, see [36] for detail. The solutions of the WENO3 and WENO4 schemes are plotted at $t = 1$ with boundary triangle size $h = \frac{2\pi}{40}$ (see Fig. 9) together with the optimal control $\omega = \text{sign}(\phi_y)$ in Fig. 14 and Fig. 15.

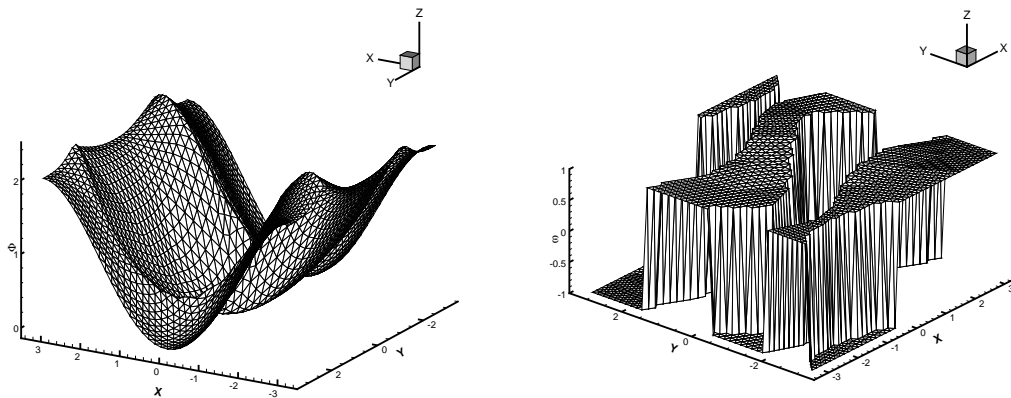


Figure 14: The optimal control problem. Boundary triangle size: $h = \frac{2\pi}{40}$. $T = 1$. WENO3 scheme. Left: the surface of the solution; right: the optimal control $\omega = \text{sign}(\phi_y)$.

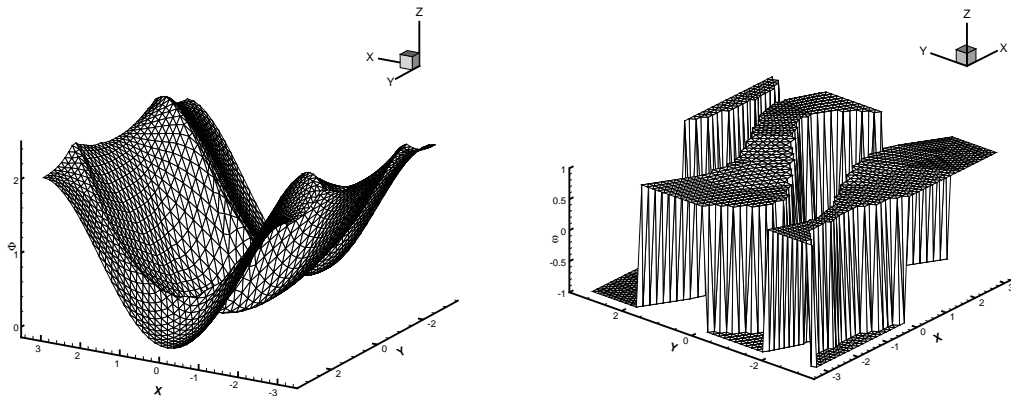


Figure 15: The optimal control problem. Boundary triangle size: $h = \frac{2\pi}{40}$. $T = 1$. WENO4 scheme. Left: the surface of the solution; right: the optimal control $\omega = \text{sign}(\phi_y)$.

Example 3.8. A two dimensional Eikonal equation with a non-convex Hamiltonian, which arises in geometric optics [23] is given by:

$$\begin{cases} \phi_t + \sqrt{\phi_x^2 + \phi_y^2} + 1 = 0, \\ \phi(x, y, 0) = \frac{1}{4}(\cos(2\pi x) - 1)(\cos(2\pi y) - 1) - 1, \end{cases} \quad 0 \leq x, y < 1, \quad (3.7)$$

The solutions of the two WENO schemes are plotted at $t=0.6$ with boundary triangle size $h=0.025$ (see Fig. 9) in Fig. 16 and Fig. 17, respectively. Good resolutions are observed with the different two WENO schemes.

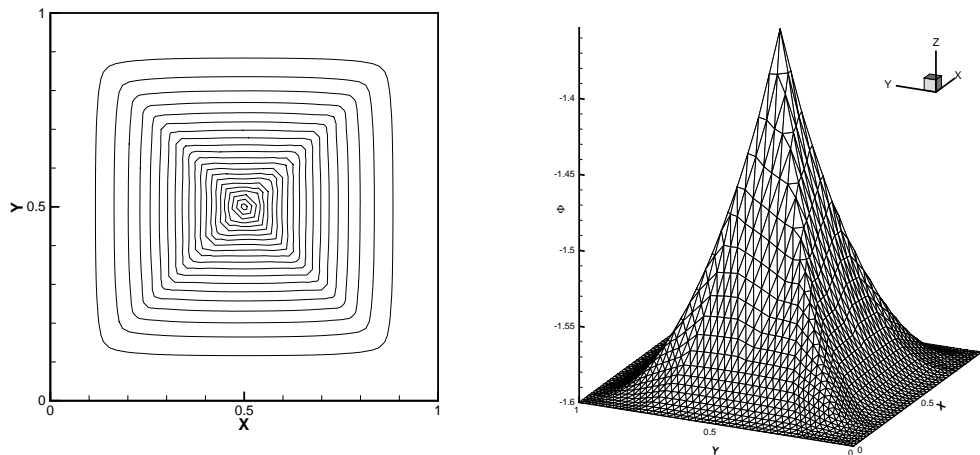


Figure 16: Eikonal equation with a non-convex Hamiltonian. Boundary triangle size: $h=0.025$. $T=0.6$. WENO3 scheme. Left: contours of the solution; right: the surface of the solution.

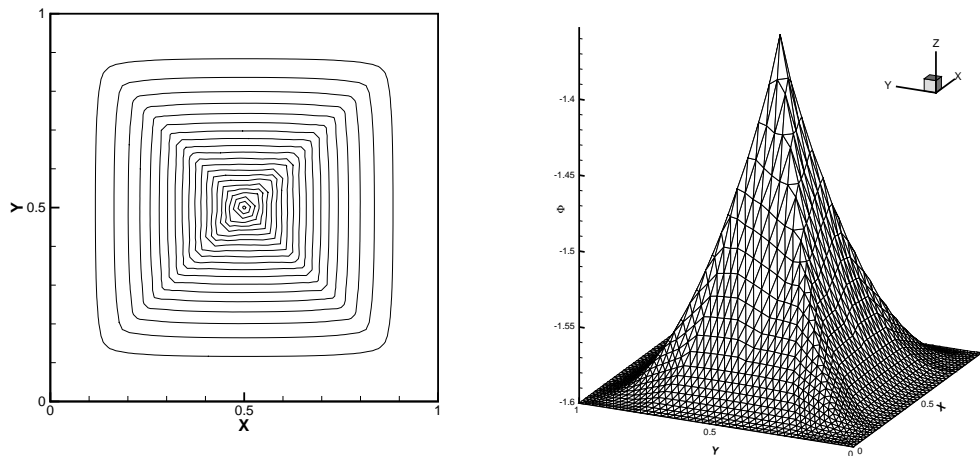


Figure 17: Eikonal equation with a non-convex Hamiltonian. Boundary triangle size: $h=0.025$. $T=0.6$. WENO4 scheme. Left: contours of the solution; right: the surface of the solution.

Example 3.9. The problem of a propagating surface [35]:

$$\begin{cases} \phi_t - (1 - \varepsilon K) \sqrt{\phi_x^2 + \phi_y^2 + 1} = 0, & 0 \leq x, y < 1, \\ \phi(x, y, 0) = 1 - \frac{1}{4}(\cos(2\pi x) - 1)(\cos(2\pi y) - 1), \end{cases} \quad (3.8)$$

where K is the mean curvature which is defined as

$$K = -\frac{\phi_{xx}(1 + \phi_y)^2 - 2\phi_{xy}\phi_x\phi_y + \phi_{yy}(1 + \phi_x^2)}{(1 + \phi_x^2 + \phi_y^2)^{3/2}},$$

and ε is a small constant. Periodic boundary conditions are used in two directions. The results of $\varepsilon = 0$ (pure convection) and $\varepsilon = 0.1$ by the WENO3 and WENO4 schemes with boundary triangle size $h = 0.025$ (see Fig. 9) are presented in Fig. 18 and Fig. 19, respectively. The surfaces at $t = 0$ for $\varepsilon = 0$ and for $\varepsilon = 0.1$, and at $t = 0.1$ for $\varepsilon = 0.1$, are shifted downward in order to show the detail of the solution at later time.

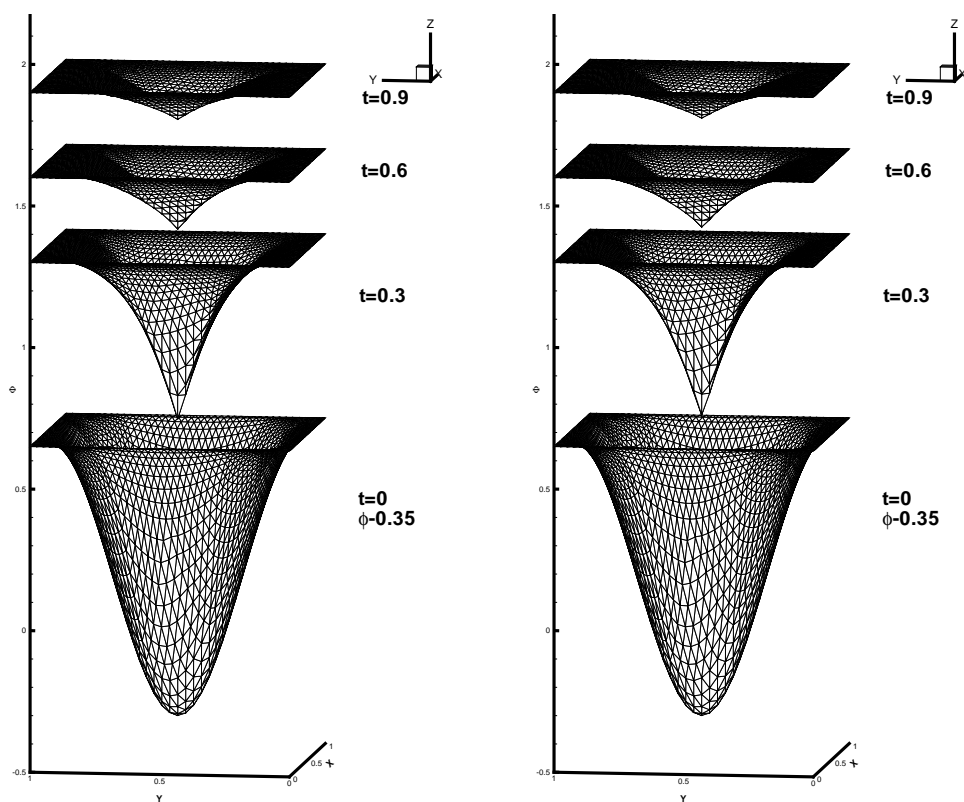


Figure 18: Propagating surface. Boundary triangle size: $h = 0.025$. $\varepsilon = 0$. Left: WENO3 scheme; right: WENO4 scheme.

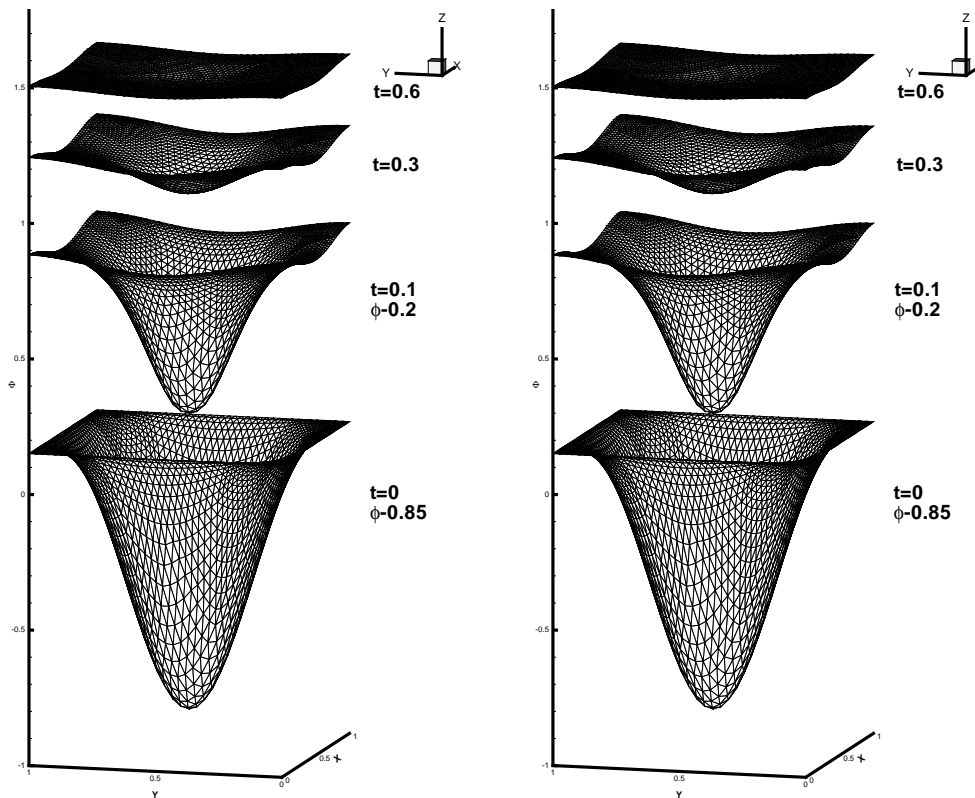


Figure 19: Propagating surface. Boundary triangle size: $h = 0.025$. $\varepsilon = 0.1$. Left: WENO3 scheme; right: WENO4 scheme.

4 Concluding remarks

In this paper we investigate designing third-order and fourth-order nodal based WENO schemes for solving the HJ equations on triangular meshes, which use a new WENO type combination of a cubic/quartic polynomial and four quadratic polynomials defined on five unequal-sized spatial stencils to obtain their x - and y -directional derivatives for obtaining high order approximations at three vertices of all triangles in two dimensions. The main advantages of such methodology are its simplicity in applying the information on only five spatial stencils and easy definition of positive linear weights with one minor constraint without taking into account the appearance of negative linear weights [44] to keep high-order accuracy in smooth regions and essentially non-oscillatory property near discontinuities. By performing such new procedures, only one big spatial stencil and four small stencils are applied in constructing different degree polynomials at associated vertices. In order to confirm the new WENO schemes converge to the optimal third-order or fourth-order accuracy in smooth regions, we modify the derivatives of high degree polynomials by subtracting four parameterized low degree polynomials which

are the derivatives of associated four quadratic polynomials. Thereafter, positive linear weights are arbitrarily chosen for these modified polynomials of different degrees based on the nodal information defined on unequal-sized stencils. Generally speaking, such new spatial reconstruction methodology is simple, effective, and could be easily extended to higher dimensions on unstructured meshes.

Acknowledgments

The research of J. Zhu is partly supported by NSFC grant 11872210, and the research of J. Qiu is partly supported by NSFC grant 11571290 and NSAF grant U1630247.

References

- [1] R. Abgrall, Numerical discretization of the first-order Hamilton-Jacobi equation on triangular meshes, *Comm. Pure Appl. Math.*, 49 (1996), 1339-1373.
- [2] R. Abgrall and T. Sonar, On the use of Muehlbach expansions in the recovery step of ENO methods, *Numer. Math.*, 76 (1997), 1-25.
- [3] S. Augoula and R. Abgrall, High order numerical discretization for Hamilton-Jacobi equations on triangular meshes, *J. Sci. Comput.*, 15 (2000), 198-229.
- [4] D.S. Balsara, T. Rumpf, M. Dumbser and C.D. Munz, Efficient, high accuracy ADER-WENO schemes for hydrodynamics and divergence-free magnetohydrodynamics, *J. Comput. Phys.*, 228 (2009), 2480-2516.
- [5] T.J. Barth and J.A. Sethian, Numerical schemes for the Hamilton-Jacobi and level set equations on triangulated domains, *J. Comput. Phys.*, 145 (1998), 1-40.
- [6] R. Borges, M. Carmona, B. Costa and W.S. Don, An improved weighted essentially non-oscillatory scheme for hyperbolic conservation laws, *J. Comput. Phys.*, 227 (2008), 3191-3211.
- [7] S. Bryson and D. Levy, High-order central WENO schemes for multidimensional Hamilton-Jacobi equations, *SIAM J. Numer. Anal.*, 41 (2003), 1339-1369.
- [8] S. Bryson and D. Levy, High-order semi-discrete central-upwind schemes for multidimensional Hamilton-Jacobi equations, *J. Comput. Phys.* 189 (2003), 63-87.
- [9] S. Bryson and D. Levy, Mapped WENO and weighted power ENO reconstructions in semi-discrete central schemes for Hamilton-Jacobi equations, *App. Numer. Math.* 56 (2006), 1211-1224.
- [10] M. Castro, B. Costa and W.S. Don, High order weighted essentially non-oscillatory WENO-Z schemes for hyperbolic conservation laws, *J. Comput. Phys.*, 230 (2011), 1766-1792.
- [11] C.K. Chan, K.S. Lau and B.L. Zhang, Simulation of a premixed turbulent flame with the discrete vortex method, *Internat. J. Numer. Meth. Engrg.*, 48 (2000), 613-627.
- [12] Y.D. Cheng and C.-W. Shu, A discontinuous Galerkin finite element method for directly solving the Hamilton-Jacobi equations, *J. Comput. Phys.*, 223 (2007), 398-415.
- [13] M.G. Crandall, L.C. Evans and P.L. Lions, Some properties of viscosity solutions of Hamilton-Jacobi equations, *Trans. Amer. Math. Soc.*, 282 (1984), 487-502.
- [14] M.G. Crandall, H. Ishii and P.L. Lions, User's guide to viscosity solutions of second order partial equations, *Bull. Amer. Math. Soc. (N.S)*, 27 (1992), 1-67.
- [15] M.G. Crandall and P.L. Lions, Viscosity solutions of Hamilton-Jacobi equations, *Trans. Amer. Math. Soc.*, 277 (1983), 1-42.

- [16] M.G. Crandall and P.L. Lions, Two approximations of solutions of Hamilton-Jacobi equations, *Math. Comput.*, 43 (1984), 1-19.
- [17] M. Dumbser and M. Käser, Arbitrary high order non-oscillatory finite volume schemes on unstructured meshes for linear hyperbolic systems, *J. Comput. Phys.*, 221 (2007), 693-723.
- [18] Y. Ha, C. Kim, Y.J. Lee and J. Yoon, Mapped WENO schemes based on a new smoothness indicator for Hamilton-Jacobi equations, *J. Math. Anal. Appl.*, 394 (2012), 670-682.
- [19] C. Hu and C.-W. Shu, A discontinuous Galerkin finite element method for Hamilton-Jacobi equations, *SIAM J. Sci. Comput.*, 21 (1999), 666-690.
- [20] C. Hu and C.-W. Shu, Weighted essentially non-oscillatory schemes on triangular meshes, *J. Comput. Phys.*, 150 (1999), 97-127.
- [21] G.S. Jiang and D. Peng, Weighted ENO schemes for Hamilton-Jacobi equations, *SIAM J. Sci. Comput.*, 21 (2000), 2126-2143.
- [22] G.S. Jiang and C.-W. Shu, Efficient implementation of weighted ENO schemes, *J. Comput. Phys.*, 126 (1996), 202-228.
- [23] S. Jin and Z. Xin, Numerical passage from systems of conservation laws to Hamilton-Jacobi equations, and relaxation schemes, *SIAM J. Numer. Anal.*, 35 (1998), 2385-2404.
- [24] A. Kurganov and E. Tadmor, New high-resolution semi-discrete central schemes for Hamilton-Jacobi equations, *J. Comput. Phys.*, 160 (2000), 720-742.
- [25] F. Lafon and S. Osher, High order two dimensional nonoscillatory methods for solving Hamilton-Jacobi scalar equations, *J. Comput. Phys.*, 123 (1996), 235-253.
- [26] O. Lepsky, C. Hu and C.-W. Shu, Analysis of the discontinuous Galerkin method for Hamilton-Jacobi equations, *Appl. Numer. Math.*, 33 (2000), 423-434.
- [27] D. Levy, S. Nayak, C.-W. Shu and Y.T. Zhang, Central WENO schemes for Hamilton-Jacobi equations on triangular meshes, *SIAM J. Sci. Comput.*, 28 (2006), 2229-2247.
- [28] D. Levy, G. Puppo and G. Russo, Central WENO schemes for hyperbolic systems of conservation laws, *Math. Model. Numer. Anal. (M²AN)*, 33 (1999), 547-571.
- [29] D. Levy, G. Puppo and G. Russo, Compact central WENO schemes for multidimensional conservation laws, *SIAM J. Sci. Comput.*, 22 (2) (2000), 656-672.
- [30] X.G. Li and C.K. Chan, High-order schemes for Hamilton-Jacobi equations on triangular meshes, *J. Comput. Appl. Math.*, 167 (2004), 227-241.
- [31] Y. Li, H. Yuan, X. Niu, Y. Yang and S. Shu, WENO Scheme-Based Lattice Boltzmann Flux Solver for Simulation of Compressible Flows, *Commun. Comput. Phys.*, 23 (2018), 1012-1036.
- [32] C.-T. Lin and E. Tadmor, High-resolution non-oscillatory central schemes for approximate Hamilton-Jacobi equations, *SIAM J. Sci. Comput.*, 21 (2000), 2163-2186.
- [33] P.L. Lions, *Generalized solutions of Hamilton-Jacobi equations*, Pitman, London, 1982.
- [34] X.D. Liu, S. Osher and T. Chan, Weighted essentially non-oscillatory schemes, *J. Comput. Phys.*, 115 (1994), 200-212.
- [35] S. Osher and J. Sethian, Fronts propagating with curvature dependent speed: Algorithms based on Hamilton-Jacobi formulations, *J. Comput. Phys.*, 79 (1988), 12-49.
- [36] S. Osher and C.-W. Shu, High-order essentially nonoscillatory schemes for Hamilton-Jacobi equations, *SIAM J. Numer. Anal.*, 28 (1991), 907-922.
- [37] J. Qiu, WENO schemes with Lax-Wendroff type time discretizations for Hamilton-Jacobi equations, *J. Comput. Appl. Math.*, 200 (2007), 591-605.
- [38] J. Qiu, Hermite WENO schemes with Lax-Wendroff type time discretizations for Hamilton-Jacobi equations, *J. Comp. Math.*, 25 (2007), 131-144.
- [39] J. Qiu and C.-W. Shu, Hermite WENO schemes and their application as limiters for Runge-

- Kutta discontinuous Galerkin method: one dimensional case, *J. Comput. Phys.*, 193 (2004), 115-135.
- [40] J. Qiu and C.-W. Shu, Hermite WENO schemes and their application as limiters for Runge-Kutta discontinuous Galerkin method II: two-dimensional case, *Comput. Fluids*, 34 (2005), 642-663.
- [41] J. Qiu and C.-W. Shu, Hermite WENO schemes for Hamilton-Jacobi equations, *J. Comput. Phys.*, 204 (2005), 82-99.
- [42] S. Serna and J. Qian, Fifth order weighted power-ENO methods for Hamilton-Jacobi equations, *J. Sci. Comput.*, 29 (2006), 57-81.
- [43] J.A. Sethian, *Level Set Methods and Fast Marching Methods*, Evolving Interface, Computational Geometry, Fluid Mechanics, Computer Vision, and Materials Science, Cambridge University Press, Cambridge, 1999.
- [44] J. Shi, C. Hu, and C.-W. Shu, A technique of treating negative weights in WENO schemes, *J. Comput. Phys.*, 175 (2002), 108-127.
- [45] C.-W. Shu, Essentially non-oscillatory and weighted essentially non-oscillatory schemes for hyperbolic conservation laws, in *Advanced Numerical Approximation of Nonlinear Hyperbolic Equations*. edited by A. Quarteroni, Editor, Lecture Notes in Mathematics, CIME subseries (*Springer-Verlag, Berlin/New York*); ICASE Report 97-65, 1997.
- [46] C.-W. Shu and S. Osher, Efficient implementation of essentially non-oscillatory shock capturing schemes, *J. Comput. Phys.*, 77 (1988), 439-471.
- [47] P.E. Souganidis, Approximation schemes for viscosity solutions of Hamilton-Jacobi equations, *J. Differ. Equ.*, 59 (1985), 1-43.
- [48] J. Yan and S. Osher, A local discontinuous Galerkin method for directly solving Hamilton-Jacobi equations, *J. Comput. Phys.*, 230 (2011), 232-244.
- [49] Y.T. Zhang and C.-W. Shu, High-order WENO schemes for Hamilton-Jacobi equations on triangular meshes, *SIAM J. Sci. Comput.*, 24 (2003), 1005-1030.
- [50] X. Zhong and C.-W. Shu, A simple weighted essentially nonoscillatory limiter for Runge-Kutta discontinuous Galerkin methods, *J. Comput. Phys.*, 232 (2013), 397-415.
- [51] J. Zhu and J. Qiu, A new fifth order finite difference WENO scheme for solving hyperbolic conservation laws, *J. Comput. Phys.*, 318 (2016), 110-121.
- [52] J. Zhu and J. Qiu, A new fifth order finite difference WENO Scheme for Hamilton-Jacobi equations, *Numer. Method Part. Differ. Equ.*, 33 (2017), 1095-1113.
- [53] J. Zhu and J. Qiu, A new type of finite volume WENO schemes for hyperbolic conservation laws, *J. Sci. Comput.*, 73 (2017), 1338-1359.
- [54] J. Zhu and J. Qiu, New finite volume weighted essentially non-oscillatory schemes on triangular meshes, *SIAM J. Sci. Comput.*, 40(2) (2018), A903-A928.
- [55] J. Zhu, X. Zhong, C.-W. Shu and J. Qiu, Runge-Kutta discontinuous Galerkin method using a new type of WENO limiters on unstructured meshes, *J. Comput. Phys.*, 248 (2013), 200-220.
- [56] J. Zhu, X. Zhong, C.-W. Shu and J. Qiu, Runge-Kutta Discontinuous Galerkin Method with a Simple and Compact Hermite WENO Limiter on Unstructured Meshes, *Commun. Comput. Phys.*, 21 (2017), 623-649.